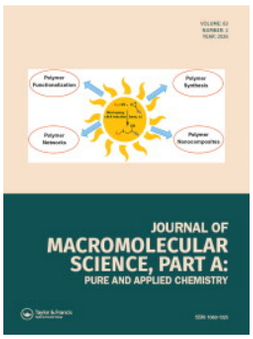

Taylor & Francis
Taylor & Francis Group

Journal of Macromolecular Science, Part A
Pure and Applied Chemistry

ISSN: 1060-1325 (Print) 1520-5738 (Online) Journal homepage: www.tandfonline.com/journals/lmsa20

Photoinitiator-dependent network restructuring in hydrogels: a mechanical, functional and biological comparison

Alime Sarikaya, Büşra Nimet Çukur, Mehtapnur Kizgin & Deniz Ceylan

To cite this article: Alime Sarikaya, Büşra Nimet Çukur, Mehtapnur Kizgin & Deniz Ceylan (2026) Photoinitiator-dependent network restructuring in hydrogels: a mechanical, functional and biological comparison, Journal of Macromolecular Science, Part A, 63:2, 157-167, DOI: 10.1080/10601325.2025.2609853

To link to this article: https://doi.org/10.1080/10601325.2025.2609853

JOURNAL OF MACROMOLECULAR SCIENCE, PART A: PURE AND APPLIED CHEMISTRY
2026, VOL. 63, NO. 2, 157–167
https://doi.org/10.1080/10601325.2025.2609853

Photoinitiator-dependent network restructuring in hydrogels: a mechanical, functional and biological comparison

Alime Sarikaya[a,b], Büşra Nimet Çukur[c], Mehtapnur Kizgin[c], and Deniz Ceylan[c]

[a]Health Sciences Institute, Department of Biotechnology, Bezmialem Vakıf University, Istanbul Türkiye; [b]Experimental Application and Research Center, Bezmialem Vakıf University, Istanbul, Türkiye; [c]Faculty of Pharmacy, Bezmialem Vakıf University, Istanbul, Türkiye

ABSTRACT

Photopolymerizable hydrogels represent a versatile class of biomaterials with tunable mechanical, structural, and biological properties. However, a comprehensive understanding of how different photoinitiators (PIs) dictate hydrogel performance remains limited. In this study, representative Type I (Irgacure 184, Irgacure 2959, TPO, LAP) and Type II (Eosin Y) PIs were systematically evaluated under identical formulation to elucidate their influence on gelation kinetics, network architecture, and cytocompatibility. Rheological, swelling, and mechanical analyses revealed that Type I initiators facilitated rapid gelation and produced highly crosslinked networks with elevated storage moduli and reduced swelling ratios. Among these, Irgacure 184 achieved the most favorable balance between stiffness and biocompatibility, whereas TPO generated the densest and stiffest networks. Conversely, the Type II Eosin Y system formed more open and hydrophilic architectures but exhibited reduced mechanical robustness due to its visible-light initiation mechanism. LAP and Irgacure 2959 demonstrated intermediate behavior, yielding moderately crosslinked, diffusion-permeable networks that supported improved cytocompatibility. Collectively, these findings highlight that PI chemistry fundamentally governs radical generation efficiency, network development, and cellular response. The mechanistic insights presented here provide a rational basis for designing photocrosslinkable hydrogels with precisely tailored structural integrity and biological performance for next-generation biofunctional materials.

GRAPHICAL ABSTRACT

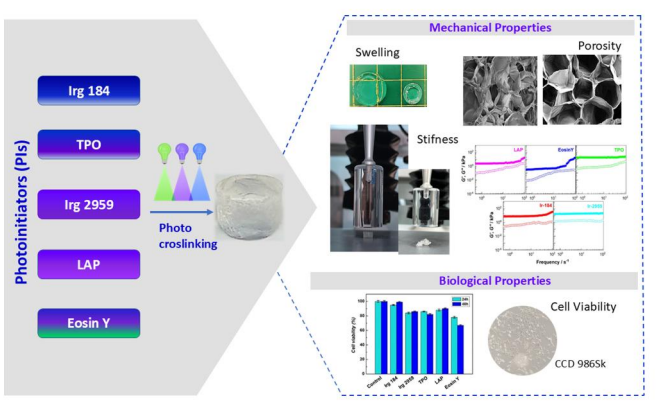

ARTICLE HISTORY
Received December 2025
Accepted December 2025

KEYWORDS
Photocrosslinkable hydrogels; photo-initiator; biocompatibility; photopolymerization; crosslinking kinetics; mechanical properties

1. Introduction

Hydrogels have emerged as an essential class of soft biomaterials owing to their high-water content, tunable mechanical properties, and remarkable biocompatibility. Their unique ability to replicate the hydrated, viscoelastic, and porous nature of the extracellular matrix (ECM) has rendered them indispensable in diverse biomedical applications, including tissue engineering, drug delivery, wound healing, and biosensing.[1–3] Among various hydrogel fabrication methods, photopolymerization-based crosslinking has become one of the most powerful and versatile techniques. This approach offers several distinct advantages, including rapid gelation, high spatial and temporal precision, and mild reaction conditions compatible with fragile bioactive molecules and living cells.[4] The efficiency and fidelity of this photocrosslinking process, however, depend primarily on the type and performance of the photoinitiator (PI) employed. The PI dictates the rate of radical formation, thereby influencing polymerization kinetics, network density, and ultimately, the mechanical robustness and biological response of the hydrogel system.[5,6]

CONTACT Deniz Ceylan deniz.ceylan@bezmialem.edu.tr Faculty of Pharmacy, Bezmialem Vakıf University, Istanbul 34093, Türkiye.

PIs are generally categorized into Type I and Type II systems according to their radical generation mechanisms. Type I PIs (e.g., Irgacure 184, Irgacure 2959, TPO and LAP) undergo unimolecular bond cleavage upon UV irradiation to directly produce radicals, yielding rapid initiation and dense crosslinking.[7] Type II PIs (e.g., Eosin Y) operate *via* bimolecular photoinduced electron- or hydrogen-transfer processes and typically require an electron or hydrogen donor co-initiator (commonly tertiary amines such as triethanolamine (TEOA) or additives like N-vinylpyrrolidone, NVP) to generate initiating radical species under visible light.[8] This indirect route, while enhancing cytocompatibility due to reduced UV exposure, often leads to lower crosslinking efficiency and diminished mechanical strength compared to Type I systems.[6]

Although some studies have evaluated individual PIs in hydrogel matrices, comparative analyses under the same experimental conditions are still lacking.[9,10] Much of the existing literature focuses on polymerization kinetics or cytotoxicity, often ignoring the integral structure-property relationships that link initiator chemistry to mechanical performance and network architecture. Furthermore, visible-light-driven photocrosslinking systems are attracting increased attention to mitigate UV-induced cell damage.[11,12] Several studies have demonstrated that differences in photoinitiator type and photolysis efficiency directly influence radical generation rates, crosslink density, and ultimately the mechanical properties of photocured polymer networks, as evidenced by UV–Vis, EPR, and real-time spectroscopic investigations.[13,14] However, the inherent balance between mechanical robustness and biocompatibility in these systems remains an unresolved and critical challenge for biomedical engineers.[15]

Given the growing demand for mechanically resilient yet cell-friendly photocrosslinkable hydrogels, understanding how different initiation pathways affect final material performance is essential. This study systematically compares hydrogels prepared with representative Type I (Irgacure 184, Irgacure 2959, TPO, LAP) and Type II (Eosin Y) PIs under standardized conditions (Table 1). We hypothesize that the initiation route dictates the balance between mechanical strength and cytocompatibility by modulating radical generation kinetics. Our results show that PI choice directly influences crosslinking efficiency, network uniformity, mechanical integrity, and cytocompatibility. Thus, PIs represent a key design parameter for engineering hydrogels that meet both mechanical and biological requirements, particularly in cell-laden or biomolecule-encapsulating systems. As 3D bioprinting advances toward more complex tissue constructs, the link between PI chemistry, crosslinking kinetics, and printability becomes increasingly important. The comparative insights from this work offer a quantitative basis for tailoring photocrosslinkable hydrogels into next-generation bioinks with improved print fidelity, structural robustness, and long-term cell viability.

Table 1. Classification of PI types and the chemical structures.

Name of PI	Type	Wavelength (nm)	Chemical Structure	Ref.
1-Hydroxycyclohexyl phenyl ketone (Irg 184)	I	200–250	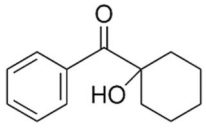	[16]
2-Hydroxy-4′-(2-hydroxyethoxy)-2-methylpropiophenone (Irg 2959)	I	320–405	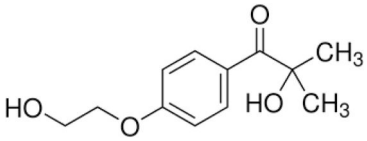	[8]
Lithium phenyl-2,4,6-trimethylbenzoylphosphinate (TPO)	I	385–420	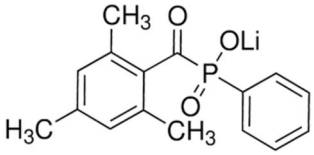	[17]
Lithium phenyl-2,4,6-trimethylbenzoylphosphinate (LAP)	I	350–410	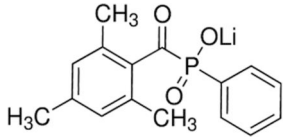	[18]
2-(2,4,5,7-tetrabromofluorescein disodium salt) (Eosin Y)	II	400–550	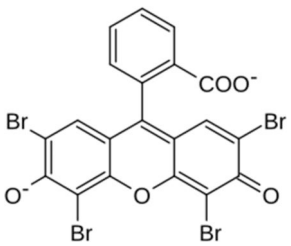	[19]

2. Materials and methods

2.1. Materials

Acrylamide (AAm; Merck), 1-vinyl-2-pyrrolidinone (VP; Merck), Triethylamine (TEA; Duzey) and poly(ethylene glycol) dimethacrylate (PEGDMA; Sigma-Aldrich) were used for hydrogel synthesis. Lithium phenyl-2,4,6-trimethylbenzoyl-phosphinate (LAP; Sigma-Aldrich), Eosin Y (supplier, Mn = 691.85 g/mol), diphenyl(2,4,6-trimethylbenzoyl) phosphine oxide (TPO; Sigma-Aldrich), 2-hydroxy-4′-(2-hydroxyethoxy)-2-methylpropiophenone (Irgacure 2959; Sigma-Aldrich), and 1-hydroxycyclohexyl phenyl ketone (Irgacure 184; Sigma-Aldrich) were employed as photoinitiators. For the cell culture studies, Trypsin/EDTA (Gibco), fetal bovine serum (FBS), DMEM/F12 medium, penicillin/streptomycin, and 3-(4,5-dimethylthiazol-2-yl)-2,5-diphenyltetrazolium bromide (MTT; Sigma-Aldrich) were purchased. Distilled water was used throughout the experiments.

2.2. Hydrogel preparation

A 0.5 mM Eosin-Y stock solution was prepared by dissolving Eosin-Y in 96% ethanol inside an amber vial and stirring at 250 rpm for 5 min. For the hydrogel precursor, Aam (≈2.8 M) and PEGDMA (100 µL, ≈18.2 mM) were dissolved in 5 mL of distilled water, followed by the addition of VP (37 mM) and TEA (100 µL, 225 mM). After incorporation of 100 µL Eosin-Y stock, the final volume was adjusted to 10 mL and the mixture was vortexed for 5 min.

For hydrogels prepared with other PIs, Aam (≈ 2.8 M) and PEGDMA (100 μL, ≈18.2 mM) were similarly dissolved in 5 mL of distilled water. The solution was transferred to an amber bottle, the desired PI was added, and the final volume was completed to 10 mL. The precursor was shaken thoroughly to ensure homogenization. Depending on the formulation, one of the following PIs was included: LAP (4 mM), TPO (2.87 mM), Irgacure 184 (4.90 mM), Irgacure 2959 (4.46 mM), or Eosin-Y (100 µL of 0.5 mM stock). For photogelation, precursor solutions were cast into cylindrical molds and irradiated with a D-Light Pro-curing system for 4–6 min. In parallel, gelation kinetics were recorded in real time on a rheometer (Anton Paar) by exposing the precursor on the rheometer plate to light for 10 min, enabling simultaneous evaluation of bulk gel formation and dynamic crosslinking behavior under standardized irradiation conditions.

2.3. Characterization of hydrogels

2.3.1. Swelling measurements

UV crosslinked hydrogels were gelled in cylindrical well molds. After gelation, cylindrical gel samples were carefully removed, weighed in their initial (post-preparation) dry state, and then immersed in distilled water at room temperature. The swelling ratio of the hydrogels was determined according to the following equation: $m_{rel} = m_t/m_0$ where m_t and m_0 represent the masses of the swollen and dry hydrogels, respectively. Swelling kinetics were monitored by weighing the gel samples separately in triplicate at predetermined time intervals until equilibrium was reached. The water medium was replenished daily to remove unreacted components and maintain sedimentation conditions. All swelling measurements were performed in triplicate to ensure reproducibility.[20]

2.3.2. Morphological analysis

The lyophilized dried gels were examined for their morphology using a high-resolution field emission scanning electron microscope (JEOL SEM-7100-EDX) operated at an acceleration voltage of 1 kV. Prior to analysis, samples were coated with Au/Pd. Elemental composition was determined by SEM-energy dispersive X-ray spectroscopy (EDX). Images were captured at several magnifications. Pore sizes were measured using the ImageJ software.

2.3.3. Gelation kinetic analysis

Gelation of hydrogel precursor solutions was initiated by UV light (Omnicure) between rheometer plates, during which the kinetics of gel formation were continuously recorded. During the measurements, the upper plate of the rheometer (15 mm in diameter) was adjusted to a gap of 0.5 mm. Rheological properties of the hydrogel networks were evaluated through frequency and strain sweep tests. The frequency sweep was conducted over a range of 0.1–100 Hz at a constant strain of 1%, while the strain sweep was performed within a range of 1%–100% at a fixed frequency of 1 Hz. The storage modulus (G′) and loss modules (G″) were used to characterize the viscoelastic behavior of the hydrogels.

2.3.4. Compression and elongation measurements

Uniaxial compression testing was performed on cylindrical hydrogel samples using the TA.XT plus Texture Analyzer (Stable Micro Systems, Surrey, UK) fitted with a 5 N load cell. Compression was applied at a constant speed of 1 mm/min using a cylindrical probe. To ensure repeatability, at least seven replicates were tested for each formulation and results were expressed as mean values. Data collection and analysis were performed using Exponent software macros.

2.3.5. Oscillatory measurements

Rheological properties were evaluated using oscillatory tests including time, frequency and strain sweeps with 15 mm parallel plates at 24 °C. A solvent trap was used to prevent evaporation, and measurements were performed in the absence of daylight. A frequency of 1 Hz ($\omega = 6.3$ rad/s) and a strain amplitude of 1% were used to ensure testing within the linear viscoelastic region (LVER). Frequency sweep tests were conducted in the range of 0.01–100 Hz immediately after gelation, while strain sweep tests were conducted at 1 Hz throughout 1%–100% strain.

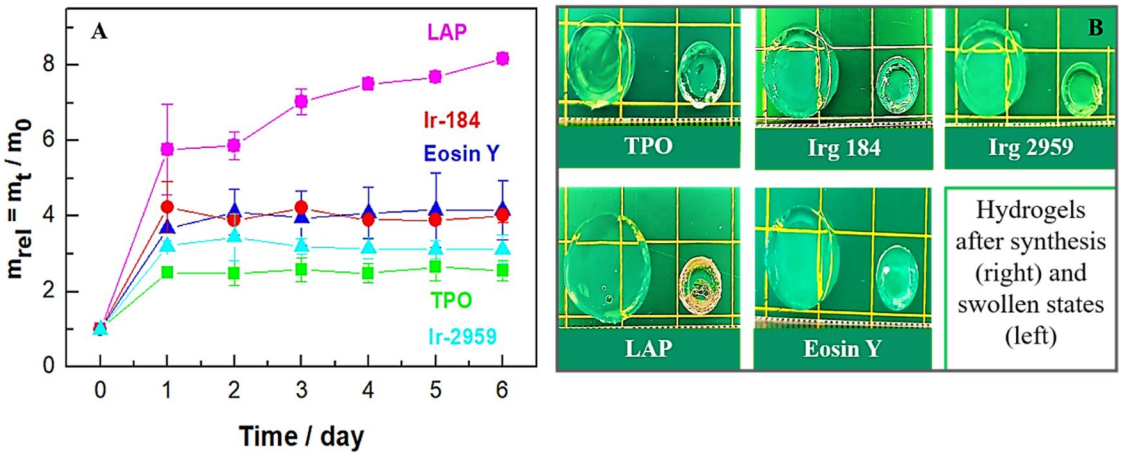

Figure 1. (A) Time-dependent relative mass swelling ratio (*m*rel) of hydrogels prepared using different photoinitiators (LAP, Irgacure 184, Irgacure 2959, Eosin Y, and TPO). Data are presented as mean ± standard deviation. (B) Representative photographs of the corresponding hydrogels after synthesis and swelling.

2.3.6. Biocompatibility assessment

In this study, human dermal fibroblast cells (CCD-986Sk; ATCC CRL-1947) were employed. Cells were maintained in T25 culture flasks using DMEM/F12 (Dulbecco's Modified Eagle Medium/Nutrient Mixture F-12), supplemented with 10% fetal bovine serum (FBS, Hyclone) and 1% penicillin-streptomycin solution (100 U/mL penicillin, 100 µg/mL streptomycin). Cultures were incubated at 37 °C in a humidified environment with 5% CO_2. Upon reaching approximately 80%–90% confluency, cells were seeded into 24-well plates and incubated for an additional 24 h. Each experimental group was tested in triplicate. Once sufficient growth was observed, the medium in each well was discarded and replaced with fresh medium. The control group consisted of wells containing only cells and fresh medium, without any material exposure. All instruments and consumables were sterilized prior to use.

To evaluate the cytocompatibility of the hydrogels, a colorimetric MTT assay was conducted after 24 and 48 h of incubation.[21] At each point, the medium exposed to the hydrogels was aspirated and replaced with fresh medium. The MTT stock solution was prepared in phosphate-buffered saline (PBS) according to the protocol originally described by Mosmann.[22] A volume of 30 μL MTT solution was added to each well, followed by gentle shaking and incubation for 2–3 h to facilitate the formation of formazan crystals. After incubation, the medium was removed, and 100 μL of dimethyl sulfoxide (DMSO) was added to dissolve the crystals. Absorbance was measured at 540 nm using a microplate reader. Cell viability was expressed as a percentage relative to the untreated control group, which was set as 100%.

3. Result and discussion

This paper presents a comprehensive evaluation of how five commonly used photoinitiators (PIs) influence the gelation behavior, mechanical properties, and biocompatibility of photocrosslinked hydrogels. Time-dependent swelling ratios ($m_{rel} = m_t/m_0$) and corresponding optical images of the hydrogels in their synthesized and swollen states are shown in Figure 1. LAP exhibited the highest equilibrium swelling, whereas TPO and Irgacure 2959 produced the lowest. Among the hydrogels, those prepared with lithium phenyl-2,4,6-trimethylbenzoylphosphinate (LAP) showed the highest equilibrium swelling ratio ($m_{rel} \approx 8$), indicating a relatively loosely crosslinked and highly hydrophilic network. In contrast, the 2,4,6-trimethylbenzoylphenyl phosphinate (TPO) and Irgacure 2959 systems exhibited significantly lower m_{rel} values, reflecting more densely crosslinked matrices that restrict water diffusion. Irgacure 184 and Eosin Y hydrogels occupied an intermediate regime: Irgacure 184 produced moderate swelling consistent with balanced network integrity, whereas Eosin Y—although less efficient in radical generation—yielded a more expanded morphology with enhanced cytocompatibility due to visible-light initiation.

The optical images corroborate these trends: LAP and Eosin Y hydrogels appear more swollen and translucent, whereas TPO- and Irgacure-based gels retain compact geometries. Overall, these findings confirm that PI chemistry directly modulates network porosity and water-uptake behavior, establishing a clear correlation between radical-generation efficiency and hydrogel swelling dynamics.

Figure 2 shows the time-dependent values of the storage (G′) and loss (G″) moduli for hydrogels fabricated using different photoinitiators under identical formulation and irradiation conditions. A rapid increase in G′, followed by its crossover and stabilization above G″, indicates the sol–gel transition and completion of network formation. Among the tested systems, LAP and TPO (Type I photoinitiators) exhibited almost instantaneous gelation within the first minute of irradiation, reflecting their high radical-generation efficiency and fast initiation kinetics. In contrast, Eosin Y (Type II) displayed only a minimal rise in G′, suggesting insufficient crosslinking under the same light intensity—likely due to its reliance on a co-initiator and susceptibility to oxygen quenching. Irgacure 184 and Irgacure 2959, also Type I initiators, showed a more gradual increase in G′ and reached plateau values at later time points compared with LAP and TPO, indicating slower but still effective network development.

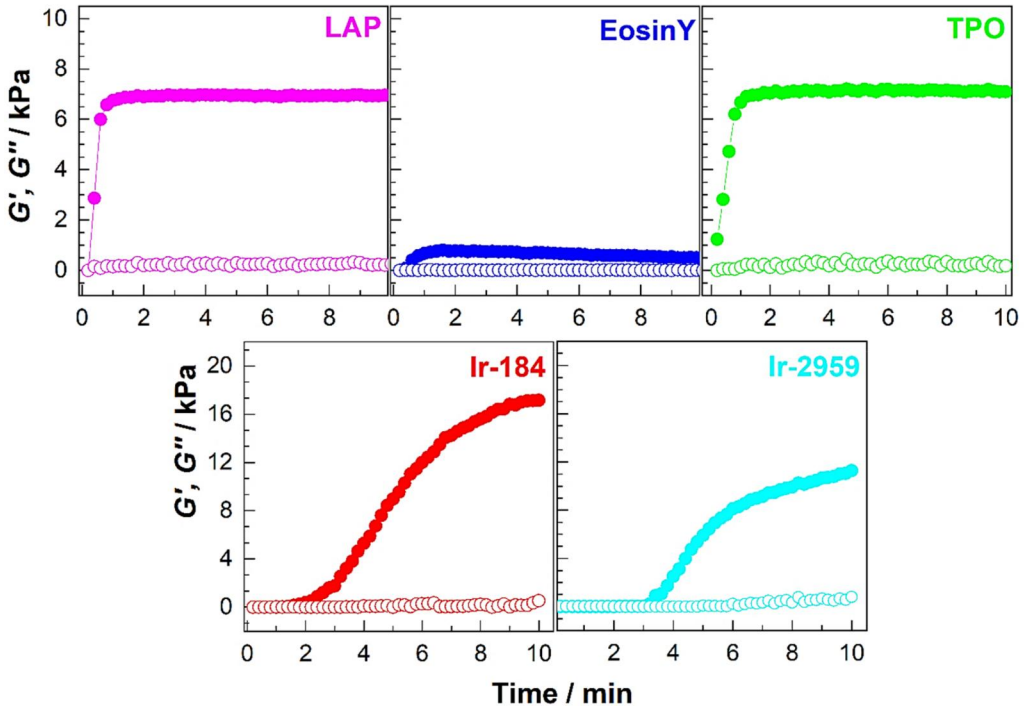

Figure 2. Time-dependent changes in storage (G′) and loss (G″) moduli during photopolymerization of hydrogels formulated with different photoinitiators (LAP, Eosin Y, TPO, Irgacure 184, and Irgacure 2959).

These rheological profiles clearly demonstrate that the radical generation mechanism governs gelation kinetics and the rate at which the polymer network forms. Type I systems, which rely on unimolecular cleavage, promote rapid and efficient crosslinking, yielding denser and mechanically stronger networks. By contrast, Type II initiation proceeds through a bimolecular mechanism and is more sensitive to oxygen inhibition, resulting in weaker and less crosslinked structures under equivalent conditions. These observations are consistent with previous reports by Holmes et al., showing that LAP-based hydrogels gel significantly faster than those initiated with Irgacure 2959 at comparable photoinitiator concentrations and irradiation intensities.[6,20,23] Similarly, the time-sweep data confirm that LAP- and TPO-crosslinked hydrogels reach the gel point (G′/G″ crossover) in under 1 min, whereas Eosin Y–based networks exhibit negligible G′ growth.

Collectively, these results confirm that the choice of photoinitiator—and thus the underlying radical generation pathway—plays a decisive role in governing gelation kinetics, crosslinking efficiency, and final hydrogel network architecture.

The frequency-dependent rheological behavior of the hydrogels is depicted in Figure 3, where G′ and G″ are plotted as a function of frequency. All samples exhibited G′ > G″ across the tested frequency range, confirming the formation of predominantly elastic, solid-like networks. However, G′ magnitude varied considerably with PI type, reflecting differences in crosslinking density and network architecture. LAP- and TPO-based hydrogels showed the highest G′ values with minimal frequency dependence, indicative of tightly crosslinked and mechanically stable networks. Hydrogels prepared with Irgacure 184 and Irgacure 2959 displayed intermediate viscoelastic responses, suggesting moderately elastic yet cohesive matrices. In contrast, Eosin Y hydrogels exhibited the lowest G′ and highest tan δ values, characteristic of more viscous and less crosslinked systems. These observations align with previous reports that Type I PIs promote faster and more homogeneous network formation, producing hydrogels with enhanced elastic moduli and long-term mechanical stability.[6] Overall, the frequency sweep data demonstrate that PI type directly dictates the viscoelastic behavior and mechanical robustness of photocrosslinked hydrogels, highlighting the mechanistic link between initiation pathway and network properties.

As shown in Figure 4, the strain-dependent changes in storage (G′) and loss (G″) moduli clearly illustrate the linear viscoelastic region (LVR) and the structural robustness of the hydrogels. Within the LVR, the constant G′ values indicate that elastic response dominates and the polymer network remains intact. Once the applied strain exceeds a critical limit, the decrease in G′ marks the onset of network breakdown and loss of structural integrity. The amplitude sweep results reveal clear differences in the mechanical behavior of hydrogels prepared with different PIs. Hydrogels crosslinked with LAP and TPO exhibited high and stable storage moduli (G′) across a broad strain range, indicating a densely crosslinked yet elastic network capable of sustaining large deformations before structural breakdown. In contrast, Eosin Y–based hydrogels showed much lower modulus values but maintained a nearly constant G′ throughout the entire strain range, resulting in a surprisingly wide linear viscoelastic region (LVR). This wide LVR, however, reflects a loosely crosslinked, highly compliant network rather than strong mechanical integrity. Irgacure 184 and Irgacure 2959 hydrogels presented the highest G′ values, consistent with

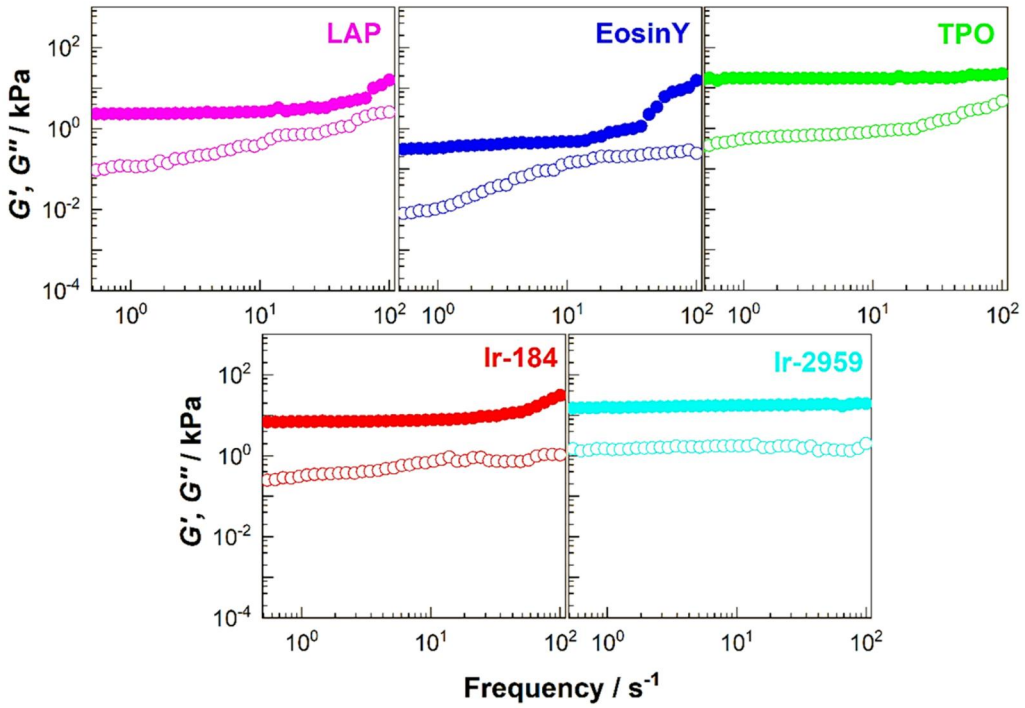

Figure 3. Frequency sweep analysis of hydrogels formulated with different photoinitiators (LAP, Eosin Y, TPO, Irgacure 184, and Irgacure 2959).

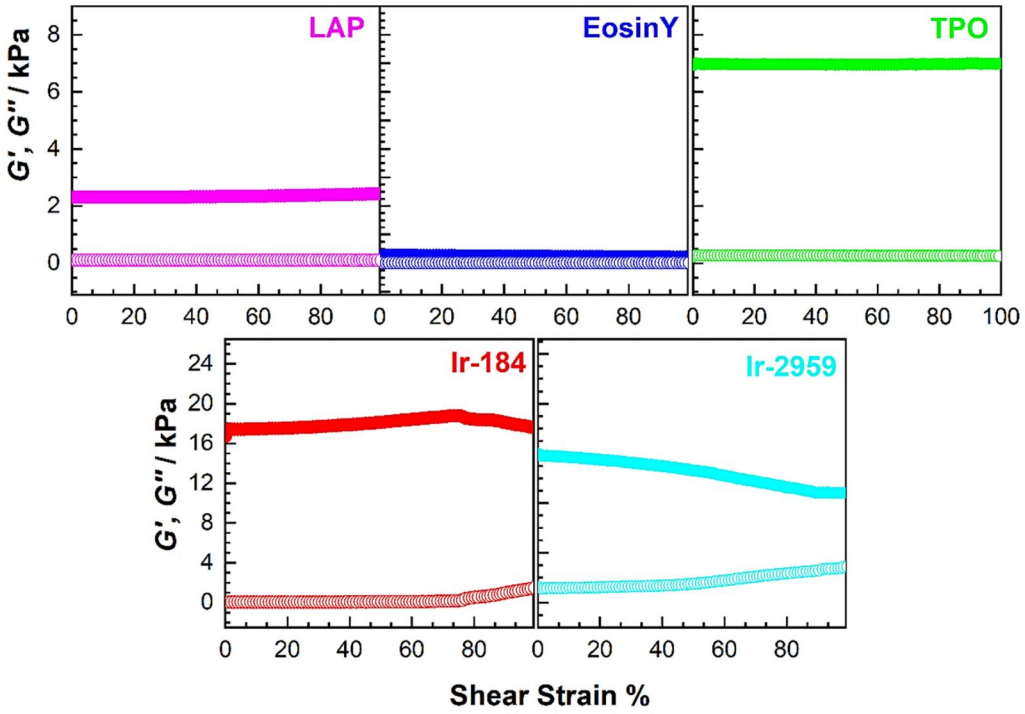

Figure 4. Amplitude sweep analysis showing the variation of storage (G′) and loss (G′′) modul of hydrogels formulated with different photoinitiators (LAP, Eosin Y, TPO, Irgacure 184, and Irgacure 2959).

stiff and highly crosslinked structures, yet they exhibited the narrowest LVR among all systems. Their early deviation from linearity suggests that although these networks are mechanically strong, they are also more brittle and less tolerant to deformation. Overall, LAP and TPO produce elastic and resilient networks, Eosin Y yields soft but highly compliant gels, and Irgacure-based systems form rigid but fragile hydrogels with limited strain tolerance.

The true stress (σ_{true}) as a function of the stretch ratio (λ) is presented in Figure 5, providing critical insight into the ultimate mechanical strength and deformation behavior of the hydrogels fabricated using various PIs. Eosin Y shows a very low small-strain modulus and can withstand large deformations in rheometer and compression tests; however, its $_{\sigma\text{true}}$–λ curve exhibits a high peak stress (~0.16 MPa). This apparent discrepancy likely arises from network

heterogeneity and differences between test modes. A low oscillatory modulus indicates a loosely crosslinked network at small strains, but localized load-bearing regions or "sacrificial bonds" may become active only at large deformations, producing a sudden peak in stress. Irg184 and Irg2959 show moderate peak stresses (~0.11 and ~0.10 MPa) with limited extensibility, consistent with more uniformly but moderately crosslinked networks. Conversely, the LAP hydrogel exhibits the lowest overall stress values ($\sigma_{true,max} \approx$ 0.035 MPa), implying the lowest mechanical robustness, likely due to the least efficient cross-linking under the identical reaction conditions. The TPO-initiated hydrogel exhibits a markedly higher Young's modulus and is considerably more brittle compared to the other formulations, indicating a stiffer yet less deformable network structure. Overall, these profiles demonstrate that the photoinitiation mechanism dictates the balance between stiffness, ductility, and large-strain behavior in photocrosslinked hydrogels.

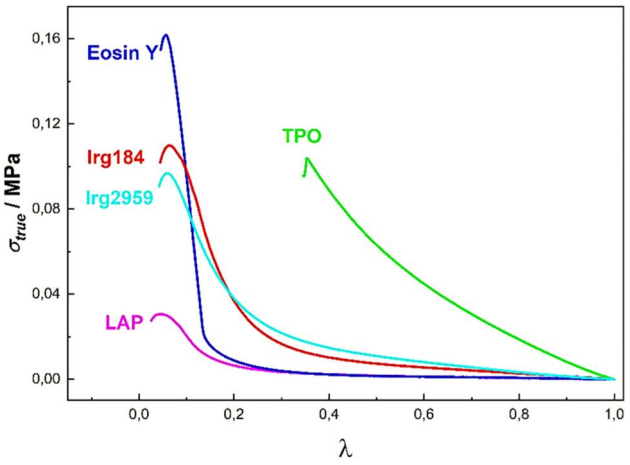

Figure 5. True stress – strain (σ_{true} vs. λ) curves for polymer networks formulated with different photoinitiators (LAP, Eosin Y, TPO, Irgacure 184, and Irgacure 2959).

The comparative analysis of bulk mechanical metrics—Young's modulus, toughness, and elongation at break—further confirms the significant impact of the PI mechanism on the final material properties (Figure 6). The Young's Modulus, a measure of material stiffness, was found to be highest for the TPO hydrogel, exceeding 100 kPa classifying it as the stiffest network structure under small strain deformation. Conversely, the LAP formulation yielded the lowest modulus, confirming it as the softest material. Regarding toughness, which quantifies the energy absorbed prior to fracture, the Eosin Y hydrogel displayed superior performance, registering the highest value (≈ 300 kJ m^{-3}). This indicates that Eosin Y generates the most mechanically resilient network, combining high strength (as observed in Figure 6) with good energy dissipation capacity. Conversely, LAP exhibited the lowest toughness. Finally, the elongation at break, which measures the material's ductility, was highest for both LAP and Irg184 hydrogels (≈25%) suggesting optimal chain flexibility within these networks. Overall, these results highlight a clear tradeoff: Eosin Y offers the highest toughness and strength at the expense of ductility, while TPO provides the highest initial stiffness, and LAP offers

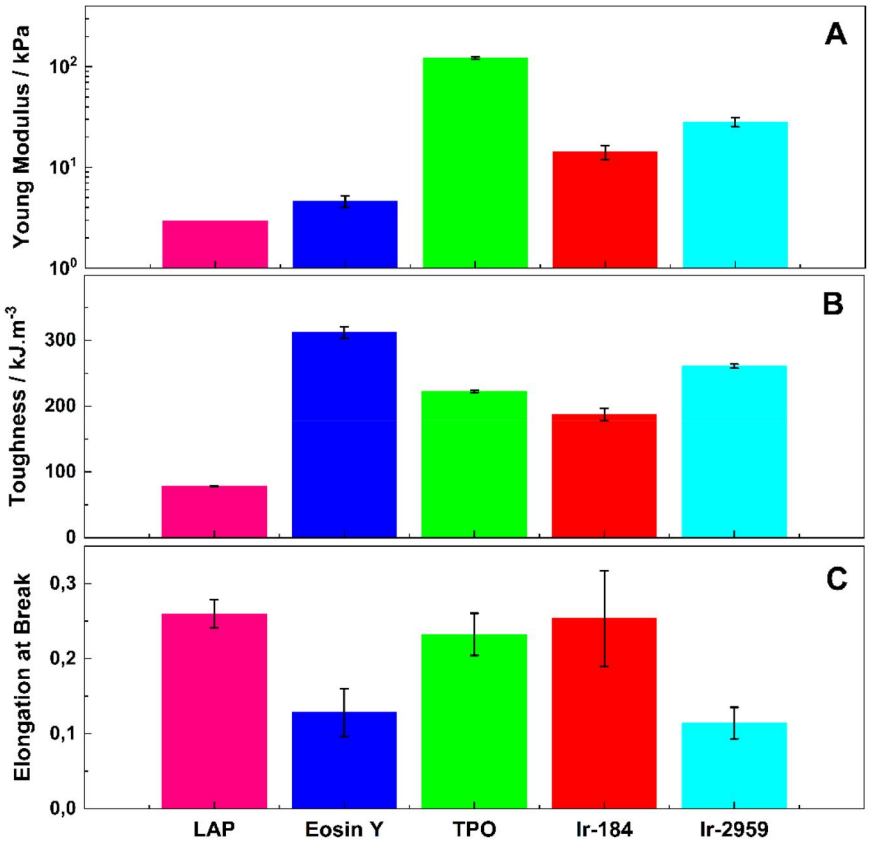

Figure 6. Mechanical properties of polymer networks formulated with different photoinitiators (LAP, Eosin Y, TPO, Irgacure 184, and Irgacure 2959): (A) Young's modulus, (B) toughness, (C) elongation at break.

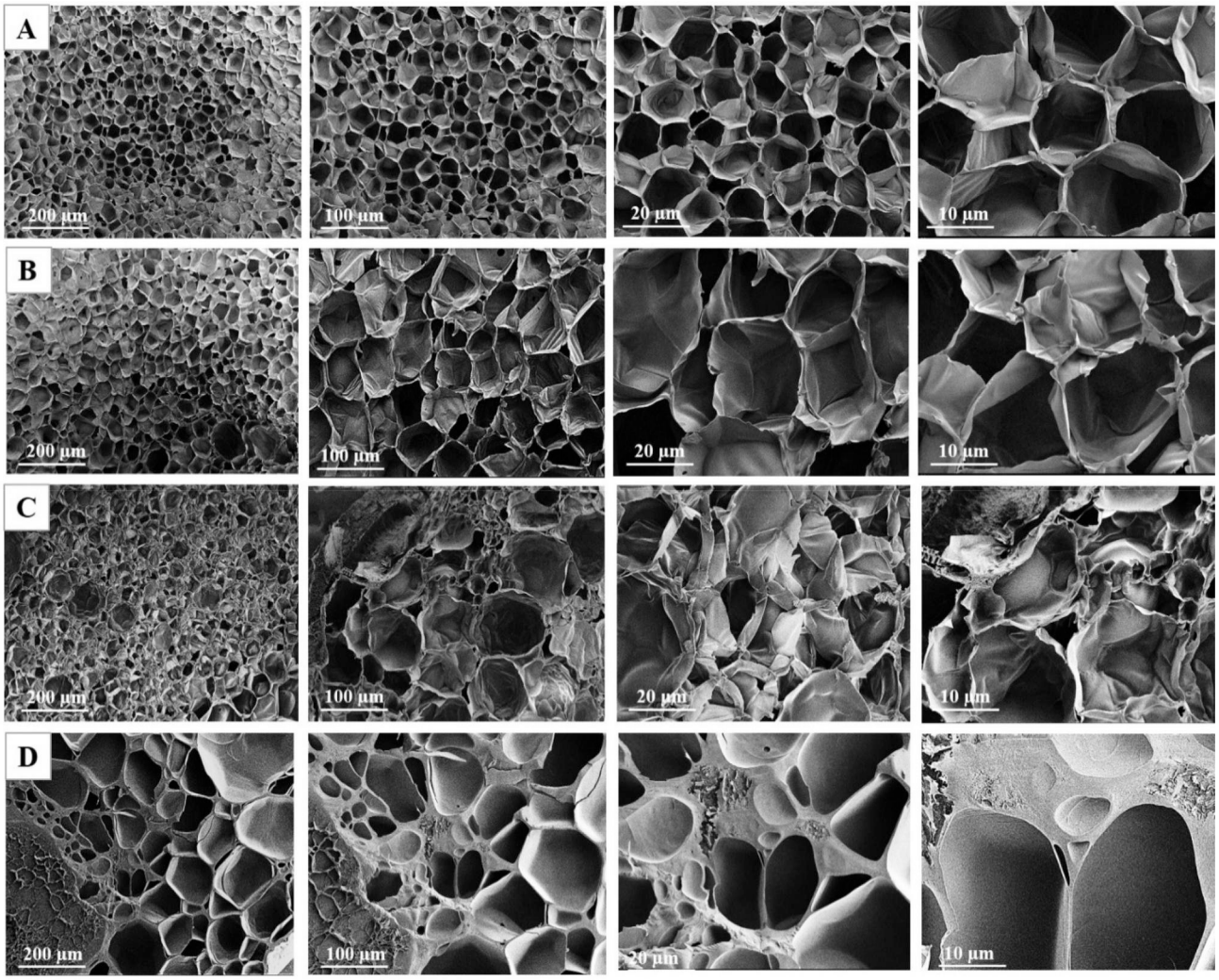

Figure 7. SEM micrographs of photocrosslinked hydrogels formulated with different photoinitiators (A) Irgacure 184, (B) Irgacure 2959, (C) TPO and (D) LAP. Scale bars (10–200 µm) are indicated on the images.

the highest elongation within the Type II group, albeit with the lowest overall strength. Quantitative mechanical analysis confirms a tradeoff between rigidity and flexibility among different PIs, emphasizing that optimal hydrogel design requires tuning radical activity to achieve desired performance.

As shown in Figure 7, the microstructural features of hydrogels prepared using different photoinitiators were evaluated by scanning electron microscopy (SEM). Hydrogels formulated with Irgacure 184 (A) exhibited dense, uniform, and highly interconnected pore structures, consistent with efficient radical generation and homogeneous crosslinking. In contrast, hydrogels prepared with Irgacure 2959 (B) displayed larger, more irregular pores and a looser network architecture, reflecting its slower photolysis and resulting in lower crosslinking density but enhanced mass transport. TPO-based samples (C) showed thick pore walls and compact, tightly packed pores, characteristic of rapid polymerization and high crosslinking density, which led to high modulus and brittle mechanical behavior. By comparison, LAP hydrogels (D) exhibited moderately open and heterogeneous pore structures, indicative of intermediate curing kinetics and crosslinking efficiency. Overall, SEM observations confirm that faster radical generation (e.g., TPO) promotes the formation of dense and mechanically robust networks, whereas slower-acting initiators (e.g., Irgacure 2959) yield more open architectures that favor diffusion, underscoring the critical role of photoinitiator selection in defining hydrogel structure–property relationships.

Overall, microstructural observations corroborate rheological and mechanical results, demonstrating that PI chemistry governs pore architecture, mechanical integrity, and biological response in photocurable hydrogels.

The MTT assay results revealed distinct cytocompatibility profiles among the hydrogels (Figure 8). Control samples exhibited nearly 100% cell viability at both 24 h and 48 h, confirming the absence of inherent cytotoxic effects from the base hydrogel matrix. Among the Type I PIs, Irg 184 demonstrated excellent biocompatibility, maintaining cell viabilities comparable to the control group (>95%), which is consistent with previous findings reporting its low cytotoxic potential and rapid photolysis into nontoxic fragments.[6,24] Irg 2959, TPO and LAP also showed acceptable cell viabilities (approximately 80%–85%), indicating moderate cytocompatibility and suitability for biomedical applications, though prolonged exposure slightly reduced viability,

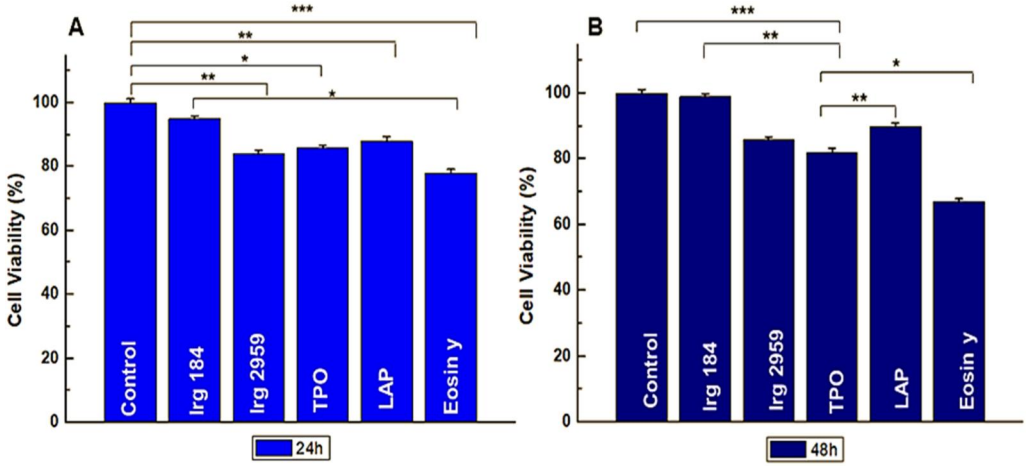

Figure 8. Cell viability (%) of human dermal fibroblasts (CCD-986Sk) assessed by MTT assay after 24 h (A) and 48 h (B) of exposure to hydrogels crosslinked with Type I (Irgacure 184, Irgacure 2959, TPO, LAP) and Type II (Eosin Y) photoinitiators (*$p < 0.05$, $n = 3$). Control samples exhibited nearly 100% viability, confirming the nontoxic nature of the base matrix.

Table 2. Rheological, mechanical, swelling, and biological properties of photocrosslinked hydrogels formulated with different photoinitiators (Irgacure 184, Irgacure 2959, TPO, LAP, and Eosin Y).

PI	Irgacure 184	Irgacure 2959	TPO	LAP	Eosin Y
G′ (kPa)	17–18	10–11	7–7.5	6.5–7	0.6–0.8
Gelation time (min)[a]	3.5–4.0	4.5–5.0	1.5–2.0	2–2.5	>5 (slow)
Young's modulus (kPa)	15 ± 2	30 ± 3	120 ± 10	3 ± 0.2	5 ± 0.3
Toughness ($kJ \cdot m^{-3}$)	190 ± 15	260 ± 10	220 ± 10	80 ± 10	310 ± 15
Elongation at break	0.25 ± 0.06	0.12 ± 0.02	0.23 ± 0.03	0.26 ± 0.03	0.13 ± 0.03
Swelling ratio (m_t/m_0)	4.1 ± 0.4	3.0 ± 0.3	2.5 ± 0.2	8.2 ± 0.3	4.1 ± 0.5
LVR stability[b]	Very high	Moderate	High	Good	Weak
Cell viability (%)	95 ± 3	85 ± 4	85 ± 3	90 ± 3	80 ± 2

All values were extracted from graphical data and are reported as approximate mean values.
Swelling ratios were taken at equilibrium (Day 6).
Mechanical parameters were obtained from compression tests.
[a]Gelation time estimated from the crossover and rapid increase of G′ during time sweep measurements.
[b]LVR stability qualitatively assessed from strain sweep behavior.

possibly due to residual radicals or incomplete polymerization byproducts. In contrast, hydrogels prepared using the Type II PI Eosin Y exhibited relatively lower cell viability, particularly for Eosin Y, for which a significant decrease (~70%) was observed at 48 h. This decrease may be attributed to the photosensitization mechanism of Type II systems, which relies on electron or hydrogen transfer with co-initiators (e.g., amines such as TEOA) and generates reactive oxygen species (ROS), potentially compromising cell integrity.[20]

The moderate cytocompatibility observed in LAP-initiated hydrogels compared to those prepared with Eosin Y can be attributed to fundamental differences in their photochemical initiation mechanisms. LAP, a Type I photoinitiator, undergoes direct homolytic cleavage upon light exposure, generating free radicals efficiently and with low susceptibility to oxygen inhibition. This direct radical generation results in faster and more uniform polymerization kinetics, reduced levels of unreacted monomers, and limited formation of reactive oxygen species (ROS), collectively contributing to improved cytocompatibility. In contrast, Eosin Y operates *via* a Type II mechanism and requires a co-initiator such as triethanolamine, a bimolecular process that is highly sensitive to dissolved oxygen. The involvement of intermediate excited states and singlet oxygen species in Type II systems often leads to increased phototoxicity and necessitates longer irradiation times to achieve complete gelation, thereby negatively impacting cell viability. Consistent with previous studies, phosphinate-based photoinitiators such as LAP have been reported to exhibit enhanced curing efficiency, higher polymerization rates, and reduced phototoxic effects in hydrogel systems.[11,25,26] Overall, these results indicate that Type I photoinitiators, particularly Irgacure 184 and LAP, provide superior cytocompatibility compared to visible-light Type II systems under the tested conditions, underscoring the critical role of photochemical pathways in defining hydrogel–cell interactions.

At 24 h, Irgacure 184 maintained cell viability comparable to the control group ($p > 0.05$), while Eosin Y, LAP, Irg2959, and TPO exhibited significantly reduced viability ($p < 0.05$). This may be explained by the cytocompatibility of Irg 184 during early photopolymerization-induced cellular stress. At 48 h, TPO exhibited lower viability compared to the other PIs ($p < 0.05$), which may be due to delayed cytotoxic effects associated with rapid radical release during polymerization. In contrast, Irg184, LAP, Irg2959, and the control group remained statistically similar ($p > 0.05$), suggesting the possibility of long-term stable cellular tolerance. Overall, Irgacure 184 maintained consistently high viability at both times, providing a favorable biological profile

compared to the others. These findings highlight the important role of photoinitiator selection in determining the short- and long-term cellular outcomes of the photocrosslinked hydrogel system.

These results highlight the importance of maintaining a delicate balance between PI efficiency and biological safety when designing photocrosslinkable hydrogels for tissue engineering applications. Selecting an appropriate initiator system requires considering not only polymerization kinetics and mechanical performance but also the overall cellular microenvironment, including oxygen concentration, light intensity, and PI concentration. Therefore, the superior performance of Irgacure 184 highlights its potential as a promising initiator for the development of biocompatible, photoreactive hydrogels designed for cell encapsulation, regenerative scaffolds, and injectable biomaterials. This conceptual model emphasizes how variations in radical formation kinetics naturally govern both the structural and biological outcomes of photocrosslinked hydrogels.

Table 2 provides a quantitative overview of photoinitiator-dependent curing behavior and the resulting rheological, mechanical, swelling, and cytocompatibility performance of the hydrogel systems, enabling a direct comparison under identical experimental conditions.

4. Conclusion

This study provides a systematic, comparative assessment of representative photoinitiators and demonstrates that variations in radical-generation kinetics critically dictate the structural, mechanical, and biological performance of photocrosslinked hydrogels. PI selection emerged not merely as a chemical choice but as a central design parameter that controls network architecture, pore morphology, crosslink density, stiffness–ductility behavior, and cytocompatibility. Among all systems, Irgacure 184 proved to be the most balanced and biocompatible initiator, forming uniformly crosslinked and cell-friendly hydrogels through efficient radical formation with minimal cytotoxic byproducts. TPO produced the stiffest and most compact networks, indicating suitability for acellular constructs or mechanically demanding applications, whereas LAP and Irgacure 2959 generated softer, more diffusion-permeable matrices that support improved metabolic activity and mass transport.

Together, these findings offer rational design guidelines for tailoring photocurable hydrogels with precise mechanical frameworks, controlled pore geometries, and optimized cell compatibility. Beyond providing fundamental insights, this work outlines a practical roadmap for engineering advanced hydrogel systems—including injectable scaffolds, adaptive biomaterial matrices, and bioinks for 3D bioprinting. By enabling deliberate modulation of structure–function relationships, the principles established here are expected to accelerate the translation of photocrosslinkable hydrogels into clinically relevant, cell-responsive, and functionally dynamic platforms for tissue repair, wound healing, and controlled therapeutic delivery.

Disclosure statement

No potential conflict of interest was reported by the author(s).

Funding

This study was financially supported by the Scientific Research Projects Committee of Bezmialem Vakif University (BAP, 20221202), Istanbul, Turkey.

References

[1] Yue, S.; He, H.; Li, B.; Hou, T. Hydrogel as a Biomaterial for Bone Tissue Engineering: A Review. *Nanomaterials* **2020**, *10*, 1511. DOI: 10.3390/nano10081511.

[2] Li, M.; Luo, A.; Luo, W.; Wang, F. Recent Progress on Mechanical Optimization of MEMS Electret-Based Electrostatic Vibration Energy Harvesters. *J. Microelectromech. Syst.* **2022**, *31*, 726–740. DOI: 10.1109/JMEMS.2022.3194859.

[3] Dhara, M. Polymer Hydrogels: Classification and Recent Advances. *J. Macromol. Sci. A* **2024**, *61*, 265–288.

[4] Fairbanks, B. D.; Macdougall, L. J.; Mavila, S.; Sinha, J.; Kirkpatrick, B. E.; Anseth, K. S.; Bowman, C. N. Photoclick Chemistry: A Bright Idea. *Chem. Rev.* **2021**, *121*, 6915–6990. DOI: 10.1021/acs.chemrev.0c01212.

[5] Groll, J.; Burdick, J. A.; Cho, D.-W.; Derby, B.; Gelinsky, M.; Heilshorn, S. C.; Jüngst, T.; Malda, J.; Mironov, V. A.; Nakayama, K.; et al. A Definition of Bioinks and Their Distinction from Biomaterial Inks. *Biofabrication* **2018**, *11*, 013001. DOI: 10.1088/1758-5090/aaec52.

[6] Fairbanks, B. D.; Schwartz, M. P.; Bowman, C. N.; Anseth, K. S. Photoinitiated Polymerization of PEG-Diacrylate with Lithium Phenyl-2, 4, 6-Trimethylbenzoylphosphinate: Polymerization Rate and Cytocompatibility. *Biomaterials* **2009**, *30*, 6702–6707. DOI: 10.1016/j.biomaterials.2009.08.055.

[7] Lang, M.; Hirner, S.; Wiesbrock, F.; Fuchs, P. A Review on Modeling Cure Kinetics and Mechanisms of Photopolymerization. *Polymers.* **2022**, *14*, 2074. DOI: 10.3390/polym14102074.

[8] Tomal, W.; Ortyl, J. Water-Soluble Photoinitiators in Biomedical Applications. *Polymers.* **2020**, *12*, 1073. DOI: 10.3390/polym12051073.

[9] Chen, Y.-C.; Kuo, Y.-T.; Ho, T.-H. Photo-Polymerization Properties of type-II Photoinitiator Systems Based on 2-Chlorohexaaryl Biimidazole (o-Cl-HABI) and Various N-Phenylglycine (NPG) Derivatives!. *Photochem. Photobiol. Sci.* **2019**, *18*, 190–197. DOI: 10.1039/c8pp00300a.

[10] Greene, T.; Lin, T. Y.; Andrisani, O. M.; Lin, C. C. Comparative Study of Visible Light Polymerized Gelatin Hydrogels for 3D Culture of Hepatic Progenitor Cells. *J. of App. Polym. Sci.* **2017**, *134*, DOI: 10.1002/app.44585.

[11] Elkhoury, K.; Zuazola, J.; Vijayavenkataraman, S. Bioprinting the Future Using Light: A Review on Photocrosslinking Reactions, Photoreactive Groups, and Photoinitiators. *SLAS Technol.* **2023**, *28*, 142–151. DOI: 10.1016/j.slast.2023.02.003.

[12] Sharifi, S.; Sharifi, H.; Akbari, A.; Chodosh, J. Systematic Optimization of Visible Light-Induced Crosslinking Conditions of Gelatin Methacryloyl (GelMA). *Sci. Rep.* **2021**, *11*, 23276. DOI: 10.1038/s41598-021-02830-x.

[13] Decker, C. Photoinitiated Crosslinking Polymerisation. *Prog. Polym. Sci.* **1996**, *21*, 593–650. DOI: 10.1016/0079-6700(95)00027-5.

[14] Voll, D.; Barner-Kowollik, C. Photoinitiators for Polymer Synthesis. Scope, Reactivity, and Efficiency. By Jean-Pierre Fouassier and Jacques Lalavée. *Angew. Chem. Int. Ed.* **2013**, *52*, 3312–3312. DOI: 10.1002/anie.201209688.

[15] Wang, X.; Xie, A.; Cao, P.; Yang, J.; Ong, W. L.; Zhang, K.; Ho, G. W. Structuring and Shaping of Mechanically Robust and

Functional Hydrogels toward Wearable and Implantable Applications. *Adv. Mater.* **2024**, *36*, 2309952. DOI: 10.1002/adma.202309952.

[16] Geisler, E.; Lecompère, M.; Soppera, O. 3D Printing of Optical Materials by Processes Based on Photopolymerization: Materials, Technologies, and Recent Advances. *Photon. Res.* **2022**, *10*, 1344–1360. DOI: 10.1364/PRJ.453338.

[17] Kowalska, A.; Sokołowski, J.; Szynkowska-Jóźwik, M. I.; Gozdek, T.; Kopacz, K.; Bociong, K. Can TPO as Photoinitiator Replace "Golden Mean" Camphorquinone and Tertiary Amines in Dental Composites? Testing Experimental Composites Containing Different Concentration of Diphenyl (2, 4, 6-Trimethylbenzoyl) Phosphine Oxide. *Int. J. Mol. Sci.* **2022**, *23*, 11594. DOI: 10.3390/ijms231911594.

[18] Gou, M.; Qu, X.; Zhu, W.; Xiang, M.; Yang, J.; Zhang, K.; Wei, Y.; Chen, S. Bio-Inspired Detoxification Using 3D-Printed Hydrogel Nanocomposites. *Nat. Commun.* **2014**, *5*, 3774. DOI: 10.1038/ncomms4774.

[19] Nachlas, A. L. Y.; Li, S.; Jha, R.; Singh, M.; Xu, C.; Davis, M. E. Human iPSC-Derived Mesenchymal Stem Cells Matured into Valve Interstitial-like Cells Using PEGDA Hydrogels. *Acta Biomater.* **2018**, *71*, 235–246. DOI: 10.1016/j.actbio.2018.02.025.

[20] Holmes, R.; Yang, X.-B.; Dunne, A.; Florea, L.; Wood, D.; Tronci, G. Thiol-Ene Photo-Click collagen-PEG Hydrogels: Impact of Water-Soluble Photoinitiators on Cell Viability, Gelation Kinetics and Rheological Properties. *Polymers* **2017**, *9*, 226. DOI: 10.3390/polym9060226.

[21] Gavanji, S.; Bakhtari, A.; Famurewa, A. C.; Othman, E. M. Cytotoxic Activity of Herbal Medicines as Assessed in Vitro: A Review. *Chem. Biodivers.* **2023**, *20*, e202201098. DOI: 10.1002/cbdv.202201098.

[22] Mosmann, T. Rapid Colorimetric Assay for Cellular Growth and Survival: Application to Proliferation and Cytotoxicity Assays. *J. Immunol. Methods.* **1983**, *65*, 55–63. DOI: 10.1016/0022-1759(83)90303-4.

[23] Nguyen, A. K.; Goering, P. L.; Reipa, V.; Narayan, R. J. Toxicity and Photosensitizing Assessment of Gelatin Methacryloyl-Based Hydrogels Photoinitiated with Lithium Phenyl-2, 4, 6-Trimethylbenzoylphosphinate in Human Primary Renal Proximal Tubule Epithelial Cells. *Biointerphases* **2019**, *14*, 021007. DOI: 10.1116/1.5095886.

[24] Bryant, S. J.; Nuttelman, C. R.; Anseth, K. S. Cytocompatibility of UV and Visible Light Photoinitiating Systems on Cultured NIH/3T3 Fibroblasts in Vitro. *J. Biomater. Sci. Polym. Ed.* **2000**, *11*, 439–457. DOI: 10.1163/156856200743805.

[25] Fairbanks, B. D.; Schwartz, M.; Halevi, A. E.; Nuttelman, C. R.; et al. A Versatile Synthetic Extracellular Matrix Mimic via Thiol-Ene Photopolymerization. *Adv. Mater.* **2009**, *21*, 5005–5010.

[26] Nguyen, K. T.; West, J. L. Photopolymerizable Hydrogels for Tissue Engineering Applications. *Biomaterials* **2002**, *23*, 4307–4314. DOI: 10.1016/s0142-9612(02)00175-8.